University of Groningen

Faculty of Mathematics and Natural Sciences

Van Swinderen Institute

Examining the effects of the magnetic field in Ba^+ ions

Bachelor Thesis

Author:
F.P.J. van Dorp

Supervisors:
prof. dr. K.H.K.J. Jungmann
dr. L. Willmann

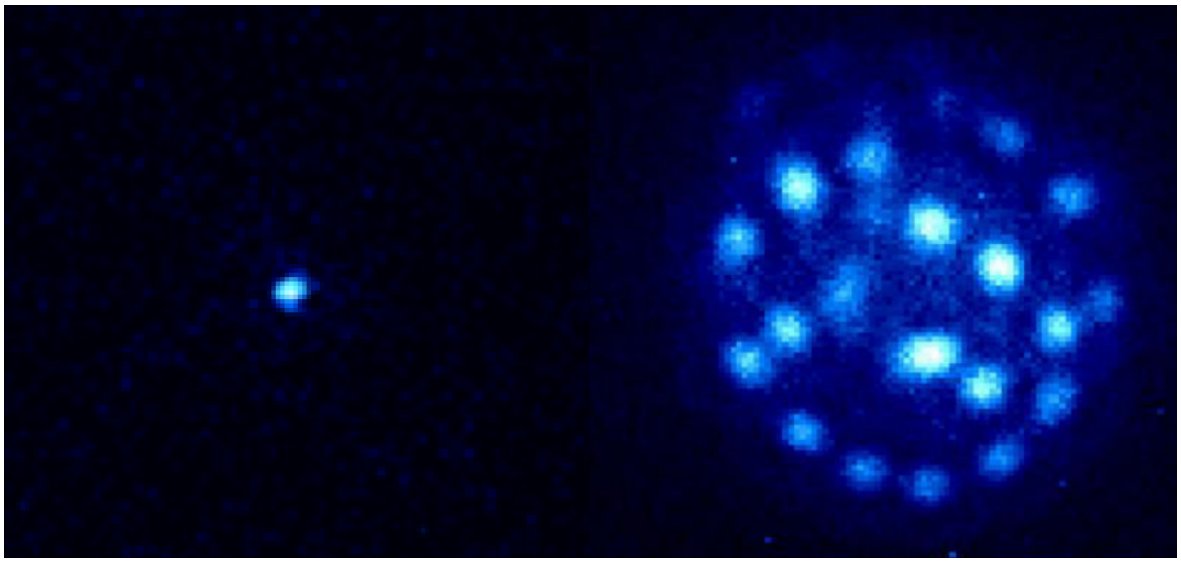

Figure 1: On the left one single trapped ion is shown and on the right an ion crystal with many ions can be seen.

July 13, 2016

Abstract

At the Van Swinderen Institute in Groningen, the Netherlands, an experiment is underway to measure the Weinberg angle sin θ_w which is a key parameter in the Standard Model. For this the light shift of energy levels in a Ba^+ ion will be determined to extract the value of sin θ_w exploiting Atomic Parity Violation. The ion is confined in a Paul trap. To determine light shift accurate knowledge of the magnetic field strength and the magnetic field direction is required. Therefore, a relation between the currents in a set of three square Helmholtz-like coil pairs around the trapped Ba^+ ion and the magnetic field induced in the x-, y- and z-direction was obtained with 1% uncertainty. The magnetic field inside the trap was calibrated by measurements at two locations outside the trap and by measurements with an ion inside the trap. Further research is required to determine this accurately. The ratio between the current on the x-coils and y-coils for a magnetic field perpendicular to the laser beams driving the $6s^2S_{1/2}$-$6p^2P_{1/2}$ and $5d^2D_{3/2}$ - $6p^2P_{1/2}$ transitions in the ion is obtained with an uncertainty of 4 %.

Contents

1 General Context

The theory in physics that explains at deepest level almost all of the phenomena that rule our daily live is 'The Standard Model of Elementary Particle Physics' or 'the Standard Model'. It describes all confirmed observations to the fundamental structure of matter and energy. It describes three of the four fundamental forces, the electromagnetic, weak and strong interactions. However, the fourth fundamental force, gravity, is not covered by this theory. This means that there must be physics beyond the Standard Model. There are two different approaches to look for physics beyond the Standard Model. The first approach is by direct production of new particles in high energy experiments. A recent example of this is the discovery of the Higgs Boson. The second approach is performing high precision experiments at low energies. An example of this is the precise measurement of Atomic Parity Violation. Such an experiment is performed at the Van Swinderen Instituut of the RUG and this thesis is in the context of this experiment. [1, 2]

1.1 Atomic Parity Violation

In the Standard Model there are three crucial discrete symmetries, namely parity P, time reversal T , and charge conjugation C. The procedure of replacing something with its mirror image is called the parity operation and this operation is described by the operator $\hat{P}$. Mathematically a parity operation means the flip of sign of a spatial coordinate, for example $\hat{P}\vec{x} = -\vec{x}$. Up to the 1950's it was assumed (without questioning) that "physics" is symmetric under each of these three discrete symmetries. But in 1957, C-S. Wu et al. [3] , proved that the weak interaction breaks the the mirror symmetry ($\hat{P}$). They studied the parity of beta-day in ^{60}Co. This experiment was quickly followed by others that confirmed parity violation and it was necessary to concede that this discrete symmetry is violated and further research was needed. [1, 4]

A description of the properties of atoms, such as their energy spectrum, can be derived from the electromagnetic (EM) interaction between the electrons and the quarks in the nucleus, caused by the exchange of massless photons between them. This process can be described by quantum electrodynamics (QED). QED is invariant under parity, so the atomic spectrum also must converse this symmetry [5]
Weak interactions also influence the physical properties of atoms, although their influence is small compared to the EM interactions. The weak interaction in atoms is mediated by the exchange of a Z^0 boson, a relatively massive particle. The Z^0 plays a role in the weak interaction between an electron and a quark in the nucleus, because it has neutral charge. Since the photons exchanged in the EM interaction are massless and the Z^0 bosons have significant mass, an EM interaction is much more probable than a short-ranged weak interaction. However, the latter does occur and this means that the electronic states of appropriate parity in the ion mix. Therefore both interactions form the electroweak interaction. A transition between two states that are forbidden by the EM selection rules can take place, as explained in the next paragraph. By investigation of the interference term of the weak force and the electromagnetic force the effect of the weak force can be measured (Figure 2). [2, 5, 6]

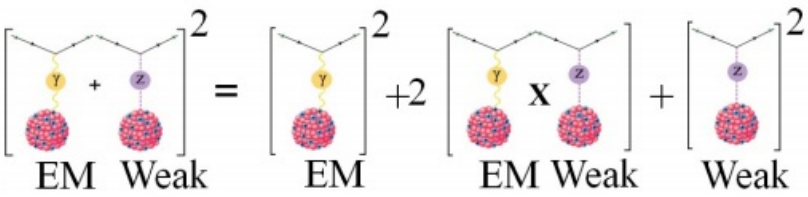

Figure 2: The interference between the electromagnetic force and the weak force. The purely weak term is too small to be detected, since the weak interaction is significantly smaller than the electromagnetic interaction. However, interference of the electromagnetic term and the electroweak term can be measured. [6]

Electric and magnetic radiation can be classified into multipoles. For electric radiation can be classified as E1+E2+E3+...+En where E1 stands for electric dipole, E2 for electric quadrupole and E3 for electric octopole. These multipoles are of the order 2^n. Radiative transitions occur according to selection rules that determine which transitions are allowed and which are forbidden. They determine for what changes in the angular quantum number l and in the magnetic quantum number m_l a transition can occur. A dipole transition can occur when the parity of the initial and final state change, Δl=($\pm$1) and $\Delta m_l = 0$ for linearly polarized light (π transition) and $\Delta m_l = \pm 1$ for circulairy polarized light (σ transition). Whenever the electric dipole transition probabilities from a given level are identically zero, we must consider the possibility of decay by electric quadrupole radiation. A quadrupole transition can occur when the parity of the initial and the final state are the same, Δl=0,$\pm$2 and $\Delta m_l = 0, \pm 1, \pm 2$ [7, 8].

In the Standard Model the mixing of the photon and the Z^0 boson is described by a single fundamental parameter, the so called weak mixing angle (Weinberg angle θ_W). It connects the coupling constant of the electromagnetic interaction, the electric charge e, with the coupling constant of the weak interaction g_W through [6]

$$sin^2(\theta_W) = \frac{e^2}{g_W^2}. \tag{1}$$

The Weinberg angle can not be measured directly, but it's possible to measure $\sin^2\theta_W$. Over a large range of energies, various experiments have determined $\sin^2\theta_W$ and other experiments are planned to determine $\sin^2\theta_W$. The results and predictions are shown in Figure 3. If the results deviate from the solid curve, which represents the value of the $\sin^2\theta_W$ as predicted by the Standard Model, it means that the Standard Model is violated and this might be explained by the existence of a dark Z boson. The dotted lines represent three possible values of the mass of such a dark Z boson.

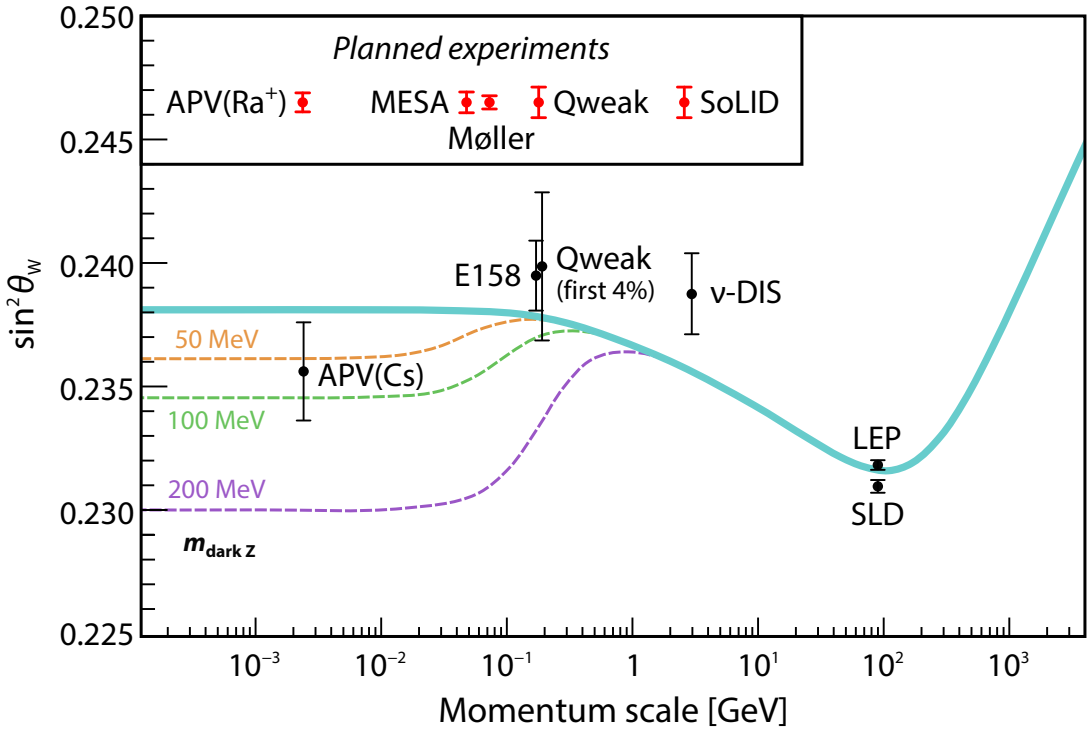

Figure 3: The Weinberg angle ($\sin^2\theta_W$) as a function of the momentum scale. The solid curve represents the value expected value of $\sin^2\theta_W$. The dashed lines are the expected values for $\sin^2\theta_W$ for different masses of a dark Z boson [2] based on [9].

1.2 Measuring APV with Barium and Radium ions.

In 1959 Y. Zel'dovich first proposed a parity violation experiment in atoms. He did this experiment with hydrogen, where the effect of APV is small and he concluded that it was of no experimental significance. But in 1974, M.A. Bouchiat and C. Bouchiat [10] calculated that the weak matrix element between $s_{1/2}$ and $p_{1/2}$ with proton number Z like

$$< ns_{1/2}|H_{APV}|n'p_{1/2} > \propto Z^2 Q_W(N,Z) K_{rel}(Z,R). \quad (2)$$

Here $< ns_{1/2}|n'p_{1/2} >$ is the overlap of the s and p atomic wave functions and H_{APV} is the Hamiltonian of the weak interaction between electrons and nucleons in an atom. The weak charge term Q_W is proportional to Z and neutron number N and the relativistic factor K_{rel} depends on Z and the radius R of the atomic nucleus. In heavy atoms the relativistic factor produces an effect such that the APV signal increases stronger than with Z^3. Therefore this relation is called the 'faster than Z^3 law'. As can been seen on the plot below, the higher the atomic number, the bigger the APV effect [2, 5].

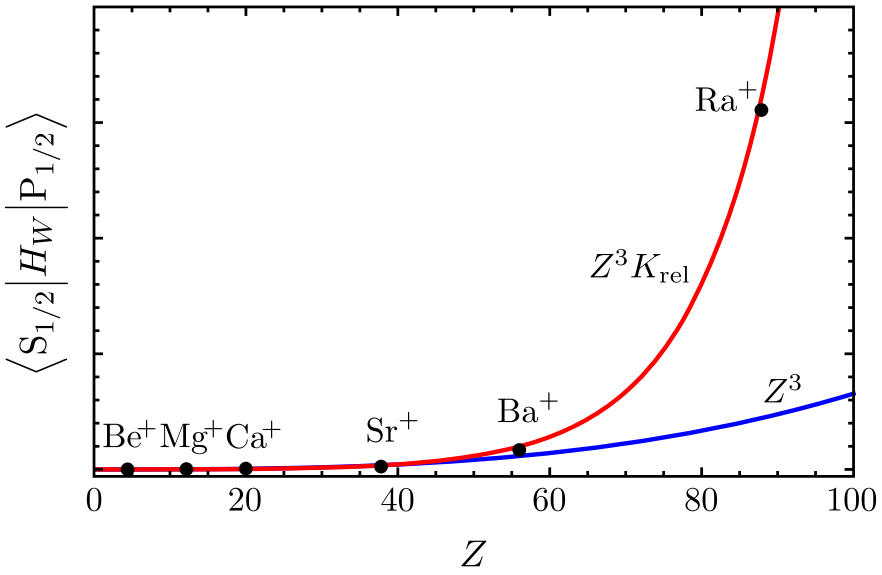

Figure 4: The scaling of the APV element for singly charged alkaline earth ions. The lower line displays the scaling with Z^3 and the upper line displays the actual scaling due to the relativistic factor K_{rel} [5].

The most accurate experiment measurement was performed with cesium, an alkali atom. Alkali atoms have the advantage that they only have one single valence electron, e.g. only one electron above a closed shell. This makes it possible to calculate the atomic wave functions to a high accuracy. The Ra^+ ion (Z=88) is the heaviest alkaline earth ion available. It is heavier than cesium and it has been shown in calculations that the APV effect is around 20 times larger for Ba^+ and around 50 times larger for Ra^+. Also there are several radium isotopes which can be employed for an APV measurement. This gives the possibility to perform ratio measurements, which reduces and even partially eliminates the uncertainties arising from the atomic physics calculations. The only disadvantage of Ra^+ is, is that Ra^+ is radioactive. Ba^+ and Ra^+ have a very similar atomic structure and therefore Ba^+ is used as precursor. The level scheme of the Ba^+ ion is shown in Figure 5. [2, 5].

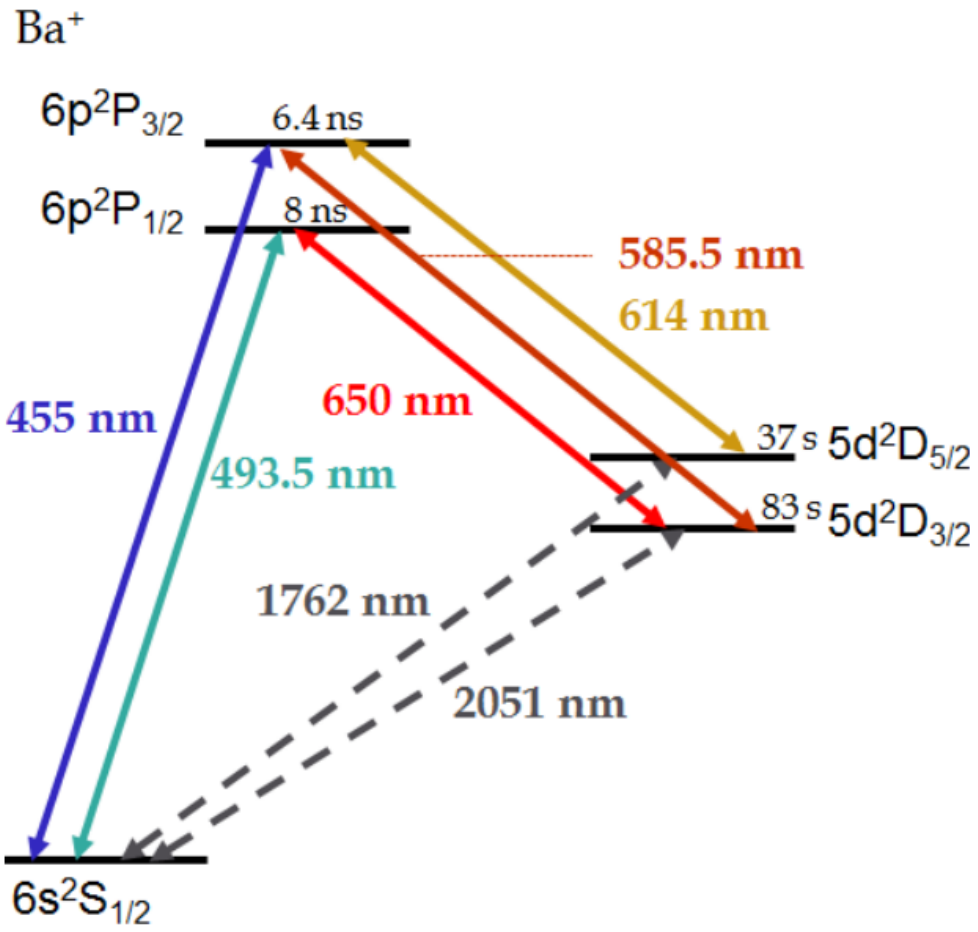

Figure 5: Level scheme of Ba^+ ion [2] based on [11].

1.3 Light Shift

In this experiment the interaction of laser light with an ion is investigated. The interaction can cause an electron to make a transition to another energy level or the energy levels themselves change. The first effect, called an on-resonant transition, arises when the light has (nearly) the same wavelength as an atomic transition from the ground state $|1\rangle$ to the excited state $|2\rangle$. Thereafter state $|2\rangle$ decays and this process continues. This causes a population transfer between two atomic levels, called Rabi oscillation. The second effect, called an off-resonant transition, is produced by intense off-resonance laser light fields that induces a light-polarization on the atom. The interaction between the laser field and the induced light-polarization causes an energy shift of the atomic energy levels, known as light shift (AC stark shift).
The light shift is described by the frequency of the transition ω_0, the frequency of the laser ω_L, the detuning $\delta{=}\omega_0{-}\omega_L$ and the Rabi frequency Ω. For a two level system the energy shift is

$$\Delta E = \pm\hbar\frac{\Omega^2}{4\delta}. \tag{3}$$

If the frequency of the laser (ω_L) is lower than the frequency of the transition(ω_0) , $\omega_L < \omega_0$, it is red-detuned and the energy difference between the states increases. If the frequency of the laser is higher than the frequency of the transition, $\omega_L < \omega_0$, it is blue-detuneed and the energy difference between the states reduces. If an external magnetic field is applied to the system, splitting of the atomic levels will occur. This phenomenon is known as Zeeman effect and the atomic levels will split into Zeeman components with energy difference ω_B (Figure 6) [2, 6, 12].

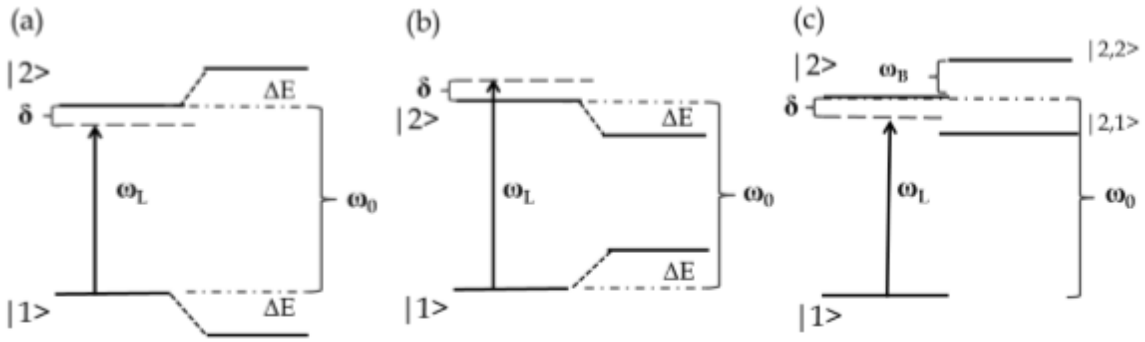

Figure 6: In (a) and (b) light shift produced by a red detuned far off-resonant laser beam and a blue detuned far off-resonant laser beam respectively and (c) Zeeman splitting of level $|2\rangle$. The Zeeman sublevels are detuned by ω_B from the resonance frequency [2]

As can be seen in Figure 7, in the presence of a magnetic field Zeeman effect causes a splitting of the degenerate fine structure states into (2j + 1) states [13]. We have a weak magnetic field, since the intern magnetic field of heavy atoms such as barium is so large compared to the applied magnetic field. For a weak magnetic field, using B to define the quantization axis field, energy shifts are linear in m_j, which runs from $m_j = -j, (-j+1), ..., (j-1), j$, and is the projection of the spin along the magnetic field direction. From [13]

$$\Delta E = g_j \mu_B B_{ext} m_j, \tag{4}$$

where $\mu_B = \frac{e\hbar}{2m_e}$ is the Bohr magneton and the Landé factor g_j is given by [13]

$$g_j = 1 + \frac{j(j+1) + s(s+1) - l(l+1)}{2j(j+1)}. \tag{5}$$

For the Barium ion, we are interested in the transitions between the $6s^2S_{1/2}$, the $6p^2P_{1/2}$ and the $5d^2D_{3/2}$ state. A Zeeman splitting will for the $6s^2S_{1/2}$ state, with l = 0, s = $\frac{1}{2}$ and j = $\frac{1}{2}$, results in two levels with Landé factor 2. The $6p^2P_{1/2}$ state, with l = 1, s = $\frac{1}{2}$ and j = $\frac{1}{2}$, this will result in two levels with a Landé factor of $\frac{2}{3}$. For the $5d^2D_{3/2}$ with l = 2, s = $\frac{1}{2}$ and j = $\frac{3}{2}$ it will result in four levels with a Landé factor of $\frac{4}{3}$ [12, 14].

To measure the light shift in an ion, a single trapped ion should be placed in the antinode of a standing wave of laser light which is resonant with the $6s^2S_{1/2}$ - $5d^2D_{3/2}$ transition. At the same time, the ion is placed at the node of another standing wave of laser light in the perpendicular direction. The intensity of the electric field is maximum at the antinode ($\vec{E}^{(i)}$), but at the node the gradient of the electric field is maximum($\vec{E}^{(ii)}$). The electric quadrupole (allowed) transition between the $6s^2S_{1/2}$ - $5d^2D_{3/2}$ states is not driven, since the ion does not see the spatial electric field gradient due to $\vec{E}^{(i)}$. It couples however the states by forbidden parity violating electric dipole transition. On the other hand, the electric quadrupole is driven because the spatial electric field gradient that is seen by the ion due to $\vec{E}^{(ii)}$.

In an external magnetic field the $6s^2S_{1/2}$ state splits into two Zeeman sub-levels. Each Zeeman sub-level undergoes a common energy shift due to the pure electromagnetic contribution, which is a scalar like AC stark shift. Due to the contribution from the interference between the weak and electromagnetic terms, the Zeeman sub-levels undergo an additional shift. This differential shift itself is a signature of atomic parity violation [6].

The differential light shift can be measured by performing radio frequency spectroscopy. A detailed description can be found in [6]. The difference in the resonant frequency, with the light shift laser turned on and off, determines the differential light shift. The frequency that corresponds to this light shift is

$$\Delta\omega = \frac{\Delta E}{\hbar} = \pm\frac{\Omega^2}{4\delta}. \tag{6}$$

This is the angular frequency, corresponding to the energy. The actual frequency change that can be measured is [15]

$$\Delta\nu = \frac{\Delta\omega}{2\pi}. \tag{7}$$

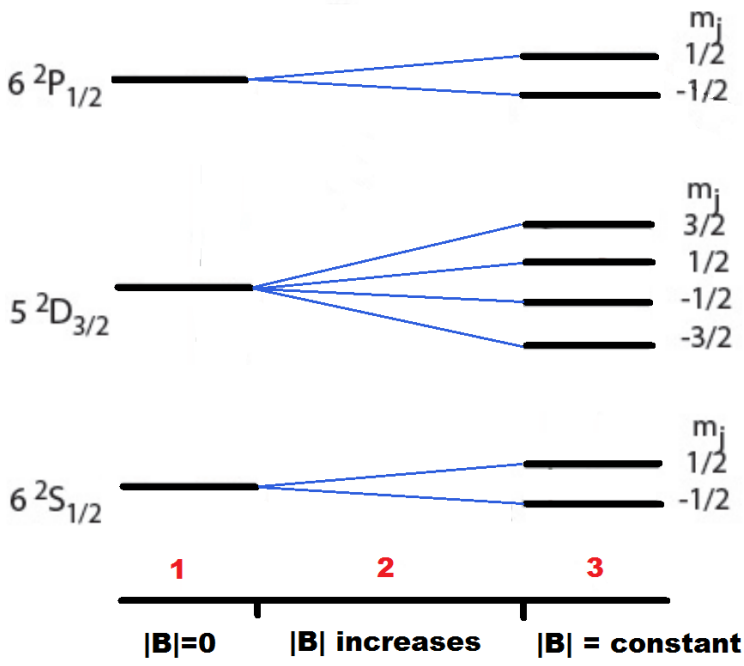

Figure 7: Schematic of the phenomenon Zeeman effect (not to scale). In region 1 the magnetic field is zero and no splitting of the energy levels takes place. In region 2 there is an increase in the magnetic field resulting in a splitting of the energy levels which is proportional to the increase in $|B|$. In region 3 a constant magnetic field is applied.

2 Experimental setup

An experiment to trap a single Ba^+ ion and to perform precision measurements has been set up. A detailed description of the experimental set up can be found in [2]. To produce barium atoms, an oven is used. The oven contains a hollow needle, filled with a mixture of Barium carbonate and zirconium powder. The oven heats the needle and a beam of barium atoms is produced. A semiconductor diode laser at 413 nm is set up to photoionizate the barium atoms into Ba+ ions. A hyperbolic Paul trap is employed to trap a single Ba^+ ion from this beam. The Paul trap is placed in a vacuum chamber with a residual gas pressure around 10^{-11} mbar. In order to keep the ion trapped, it needs to be cooled by light from two lasers. A dye laser and a frequency doubled Ti:Sapphire laser are used for this purpose. To keep the frequency of the lasers stable, the dye laser is locked to a iodine locked diode laser and the Ti:Sapphire laser is locked to light of a frequency comb. These lasers are also used to perform laser spectroscopy. An Electron Multiplying CCD (EMCCD) camera is used to get an image of the trapped ion and a photo multiplier tube (PMT) is used to detect photons. A Data Aqcuistion Program (DAQ) has been set up to collect all the data from the experiments. The vacuum chamber is placed inside three pairs of rectangular Helmholtz-like coils arranged in a cubical geometry to generate an adjustable magnetic field $\vec{B}$.

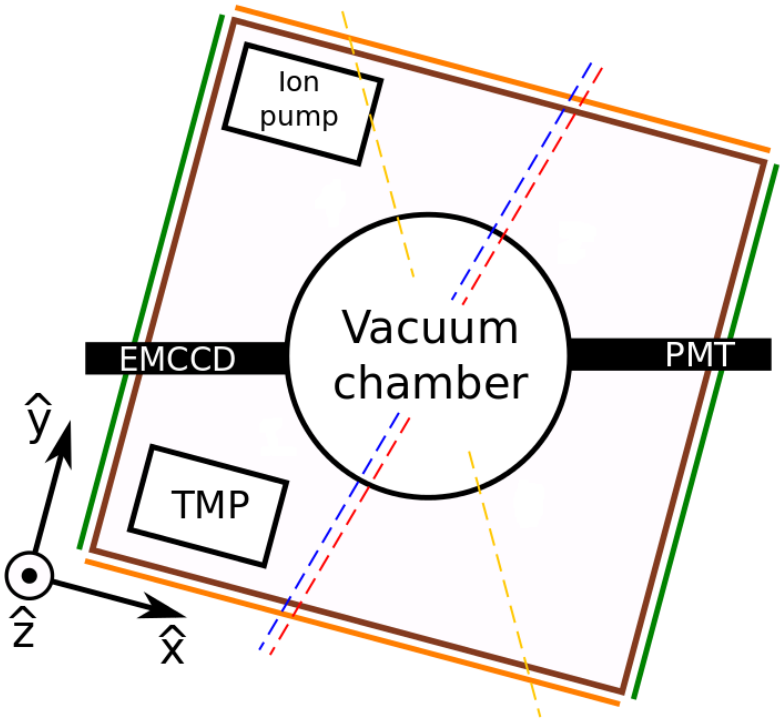

Figure 8: Schematic description (top view) of the experimental set up. PMT stands for Photo Multiplier Tube and EMCCD for Electron Multiplying CCD and both are used for the imaging of the ions. The yellow line is the light shift laser, the blue and red laser beams are for the cooling of the ion and the laser spectroscopy. The green and yellow lines indicate the rectangular current coils [16].

2.1 Lasers

Lasers are devices that generate or amplify light[17]. The word laser is an acronym for 'light amplification by stimulated emission of radiation'. Lasers come in a great variety of forms and the beams that lasers emit or amplify have remarkable properties of directionality, spectral purity and intensity. The essentials of a laser device are: (i) a laser medium, or gain medium, consisting of an appropriate collection of atoms, molecules, ions or electrons in a semiconducting crystal; (ii) a pumping process to excite the atoms (molecules, etc) of the laser medium into higher energy levels; and (iii) suitable optical feedback elements that allow a beam of radiation to bounce back and forth repeatedly through the laser medium (as in a laser oscillator).

In the laser medium (i), a transition from a higher level energy state to a lower level energy state can occur by spontaneous emission and by stimulated emission. Spontaneous emission happens when a photon spontaneously is released when a transition from a higher level to a lower level and produces fluorescence light at the transition frequency, emitted in a random direction. Stimulated emission occurs when a photon induces a transition from a higher level to a lower level. The photon that induces the transition and the photon that is emitted in this transition will have the transition frequency and the same direction. These induced transitions will create the laser light.
The pumping process (ii) is required to excite atoms into their higher quantum-mechanical energy levels. For laser action to occur, a condition of population inversion has to be fulfilled. Population inversion means that population of the higher energy levels is greater than the population of the lower energy levels. This can be achieved by a so called four-level system (see figure below). In a four-level laser, the atoms are pumped from the ground state(level 0) to a high excited state(level 3). The atom decays rapidly to level 2. The decay from level 2 to level 1 must be a relatively slow process in order to obtain population inversion. This is the decay where the laser light is emitted. The decay from level 1 to level 0 must be a fast process again. Since the decay from level 2 to level 1 is a lot slower than the other two decays, population inversion is achieved (Figure 9).
The feedback in a laser oscillator, or a cavity, is formed by mirrors at each end of the amplifying laser medium. In this way, the photons can bounce back and forth between these mirrors. This increases the chance that stimulated emission is induced. By placing a partially emitting mirror on either end, some of the photons will go through the mirror and laser light is produced.

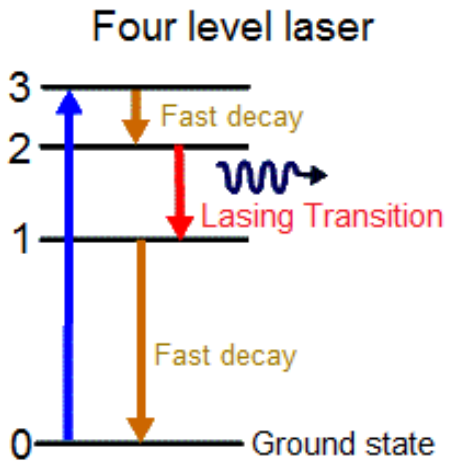

Figure 9: The pumping process to obtain population inversion. The atoms are pumped from the ground state (level 0) to the high excited state (level 3). Subsequently it decays fast to level 2. The decay from level 2 to level 1 is relatively slow in order to create population inversion. The decay from level 1 back to the ground state is fast again. (adapted from [18])

2.2 Detection and laser cooling

Light of two lasers is used to cool the ion and perform laser spectroscopy. For the cooling, the $6s^2S_{1/2}$-$6p^2P_{1/2}$ transition with wavelength 493.5 nm and the $5d^2D_{3/2}$-$6P^2P_{1/2}$ transition with wavelength 650 nm need to be driven. For the $5d^2D_{3/2}$-$6P^2P_{1/2}$ transition, a Coherent CR-699 ring dye laser is used. To stabilize the frequency of the dye laser, it is locked to a stabilized diode laser. The diode laser is stabilized by referencing the frequency of the light from the diode laser to a specific transition in iodine (I_2). Since the transitions of molecular I_2 are known very precise, this transition has been determined to 1 MHz accuracy [19], iodine is a perfect candidate for this. A specific transition in I_2 is used as a lock point to the wavelength of the diode laser.
Laser light at a wavelength 987 nm from a single-frequency Ti:Sapphire laser is frequency doubled for the $6s^2S_{1/2}$-$6p^2P_{1/2}$ transition. In order to have stable laser cooling a frequency control of order of 1 MHz is essential. Therefore frequency of the Ti:Sapphire laser is locked to a frequency comb[2]. A detailed description about the frequency comb can be found in [20]. The light of the Ti:Sapphire laser is compared with light from the frequency comb. When both the wavelengths match, a beatnote signal can be seen. The frequency of the laser can be locked to the frequency of the frequency comb and the frequency comb can be used to control wavelength of the laser [2].

3 Measurements of the magnetic field

In the presence of a magnetic field splitting of the atomic levels will occur due to Zeeman effect. This influences the atomic transitions in the barium ion (see section 1.3). Good knowledge of the of the magnetic field at the location of the ion is required to explain and predict this influence. Therefore, different experiments regarding the magnetic field have been performed.
The magnetic field is generated by a set of rectangular coil-pairs in Helmholtz-like geometry in all three orthogonal directions. If a current is run through the coils, a homogeneous magnetic field is induced [21]. The magnitude and strength of the magnetic field depends on the current that is flowing through the coils. The first measurement is conducted to obtain a relationship between the generated magnetic field and the current run through the coils and to determine the background magnetic field at the position of the barium ion. The second measurement is done to determine the behavior of the gradient of the magnetic field in the z-direction. The third measurement is executed to determine the background magnetic field in a more accurate way. The fourth measurement is conducted to obtain the ratio between the current on the coils in order to get the resulting magnetic field perpendicular to the Ti:Sapphire and the dye laser beams.

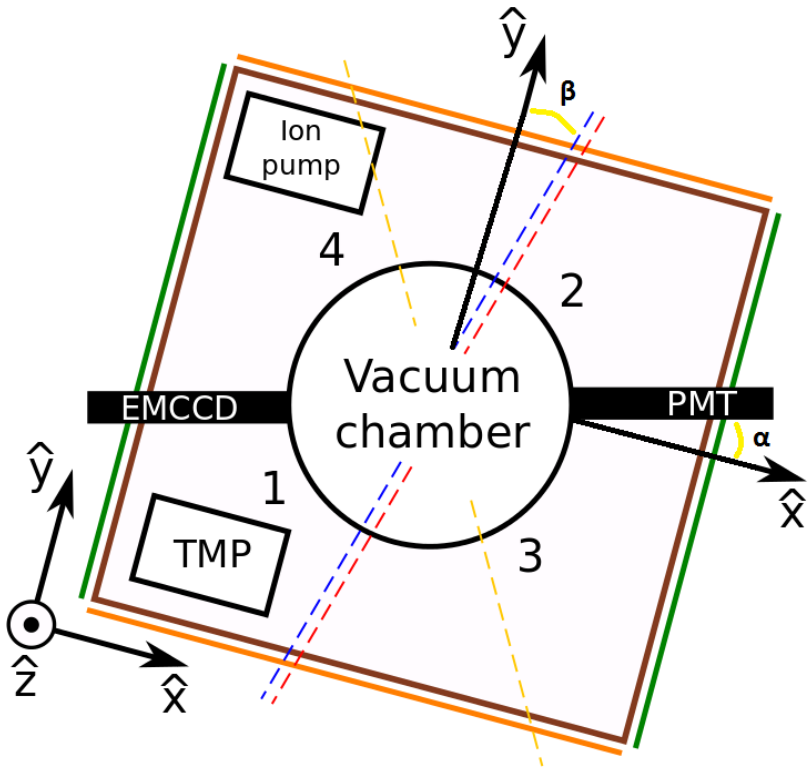

Figure 10: Schematic description (top view) of the experimental set up. PMT stands for Photo Multiplier Tube and EMCCD for Electron Multiplying CCD and both are used for the imaging of the ions. The yellow line is the light shift laser beam, the blue and red laser beams are for the cooling of the ion and the laser spectroscopy. The green and yellow lines indicate the rectangular current coils. The numbers 1,2,3 and 4 indicate the positions at which several measurements on the magnetic field were conducted. The angles α and β are between the x-axis and the EMCCD/PMT as well as the y-axis and the direction of the Ti:Sapphire and dye laser beams respectively [16].

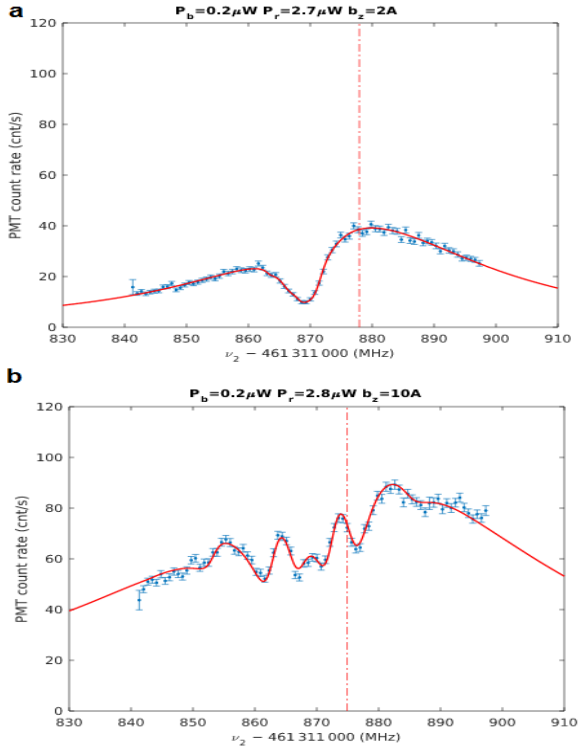

Figure 11: Spectrum measured for the $6s^2S_{1/2}$- $6p^2P_{1/2}$ transition with one trapped ion while scanning the frequency of the dye laser. The detuning of the Ti:sapphire laser is fixed at the position of the red vertical line and the power of the laser beams are shown for each plot. The magnetic field induced by the coil pairs is pointed in the z-direction and is approximately 150 μT for (a) and 750 μT for (b). Dips in the spectra correspond to two-photon transitions between the $6s^2S_{1/2}$ state and the $5d^2D_{3/2}$ state. These dips appear if the frequency detuning is the same for both lasers. In (a) the Zeeman splitting of the energy levels is small, therefore the two-photon transitions occur between different Zeeman sublevels of the $6s^2S_{1/2}$ state and the $5d^2D_{3/2}$ state can not be distinguished and only one dip appears. In (b) multiple dips are shown and each dip corresponds to a specific two-photon transitions between different Zeeman sublevels of the $6s^2S_{1/2}$ state and the $5d^2D_{3/2}$ state [22].

The influence of the magnetic field on the transitions between the $6s^2S_{1/2}$, $6p^2P_{1/2}$ and $5d^2D_{3/2}$ can be illustrated by the figure above. Laser spectroscopy has been conducted for two different magnetic fields. The detuning of Ti:Sapphire laser is fixed and the detuning of the dye laser is scanned near resonance. In Figure 11a a current of 2A is put on the coils in the z-direction. This corresponds to a magnetic field of approximately 150 μT in the z-direction. In Figure 11b a current of 10A is put on the coils in the z-direction, corresponding to a magnetic field of approximately 750 μT in the z-direction. The fluorescence signal is collected by the PMT from emitted photons of the $6s^2S_{1/2}$-$6p^2P_{1/2}$ transition in the trapped Ba^+ ions. The dips in the spectra appear if the frequency detuning is the same for both lasers. Then the two-photon Raman transition between the $6s^2S_{1/2}$ state and the $5d^2D_{3/2}$ state is driven [2]. In Figure 11a only one dip is observed and in Figure 11b multiple dips are shown. Zeeman splitting of the energy levels scales linearly with the external magnetic field (equation 9). If the external magnetic field is low, as is the case in Figure 11a, the energy splitting of the $6s^2S_{1/2}$ and the $5d^2D_{3/2}$ states is small. The two-photon transitions occur between different Zeeman sublevels of the $6s^2S_{1/2}$ state and the $5d^2D_{3/2}$ state. Since the Zeeman sublevels are so close to each other, these transitions occur at nearly the same frequency of the dye laser and only one dip is observed. In Figure 11b, multiple dips are observed, corresponding to two-photon transitions between the different Zeeman sublevels of the $6s^2S_{1/2}$ state and the $5d^2D_{3/2}$ state. The two-photon transitions between the different Zeeman sublevels of the $6s^2S_{1/2}$ state and the $5d^2D_{3/2}$ state occur for different detunings of the dye laser. This can be observed in the different dips.

3.1 Calibrating the magnetic field at the position of the ion by external measurements

In our experimental set up, different components contribute to the magnetic field at the place of the ion, e.g. the earth magnetic field and other magnetic components. The goal of this experiment is to determine the back ground magnetic field at the position of the ion and to determine how much current on the rectangular Helmholtz coils is needed to compensate this.
The magnetic field at the place of the ion was determined by measuring x, y and z component of the magnetic field with a Gaussmeter for different values for the current at two locations on opposite sites outside the vacuum chamber. Initially this was supposed to be measured at four locations, but since the ion pump influenced the magnetic field at location 4 (see Figure 10), we decided to measure the magnetic field only at location 1 and 2. We assumed the magnetic field scaled linearly between those two points.
A probe holder was installed at location 1 and 2, so that the magnetic field would be measured at the same location. The current was varied on each of the axes between 5 A and -5 A with intervals of 1A, while the current ran through the coils in the other directions canceled the magnetic field in the other directions. A Matlab script was written to plot the data.

The magnetic field depended linearly on the current, but the dependence for location 1 and 2 was different. Assumed was that the magnetic field between the two locations scaled linearly, so the average of the two functions for each of the magnetic field directions was determined. The functions are given in μ T, where 1 G = 100 μ T

$$B_x(I_x) = 5.52(3) \cdot 10^1 \mu T/A \cdot I_x - 0.16(3) \cdot 10^1 \mu T, \tag{8}$$

$$B_y(I_y) = 5.72(3) \cdot 10^1 \mu T/A \cdot I_y + 0.54(3) \cdot 10^1 \mu T, \tag{9}$$

$$B_z(I_z) = 7.60(3) \cdot 10^1 \mu T/A \cdot I_z - 3.95(3) \cdot 10^1 \mu T. \tag{10}$$

The uncertainty in the functions above and in Figure 12 are derived from the reading error in the Gaussmeter combined with its intrinsic accuracy. From these functions the current needed to compensate the external magnetic field in the three directions was determined.

$$I_x = 2.9 \cdot 10^{-2} A, \tag{11}$$

$$I_y = -9.4 \cdot 10^{-2} A, \tag{12}$$

$$I_z = 5.2 \cdot 10^{-1} A. \tag{13}$$

The error in the current is neglectable. The total magnetic field is given by

$$|B| = \sqrt{(B_x^2 + B_y^2 + B_z^2)}. \tag{14}$$

Inserting the values of the magnetic field at zero current from (9), (10) and (11) gives

$$|B| = 4.00(5) \cdot 10^1 \mu T. \tag{15}$$

From (4), (6) and (7) follows that the frequency shift due to Zeeman effect is given by

$$\Delta\nu = \frac{g_j \mu_B B_{ext} m_j}{h}. \tag{16}$$

For the $6s^2S_{1/2}$ state this results in a frequency shift of $\Delta\ \nu = 0.56$ MHz
For the $6p^2P_{1/2}$ state this results in a frequency shift of $\Delta\ \nu = 0.19$ MHz
For the $5d^2D_{3/2}$ state this results in a frequency shift of $\Delta\ \nu = 0.37$ MHz for $m_j = \pm\ \frac{1}{2}$ and a frequency shift of $\Delta\ \nu = 1.1$ MHz for $m_j = \pm\ \frac{3}{2}$.
The errors in the frequency shift are neglectible.

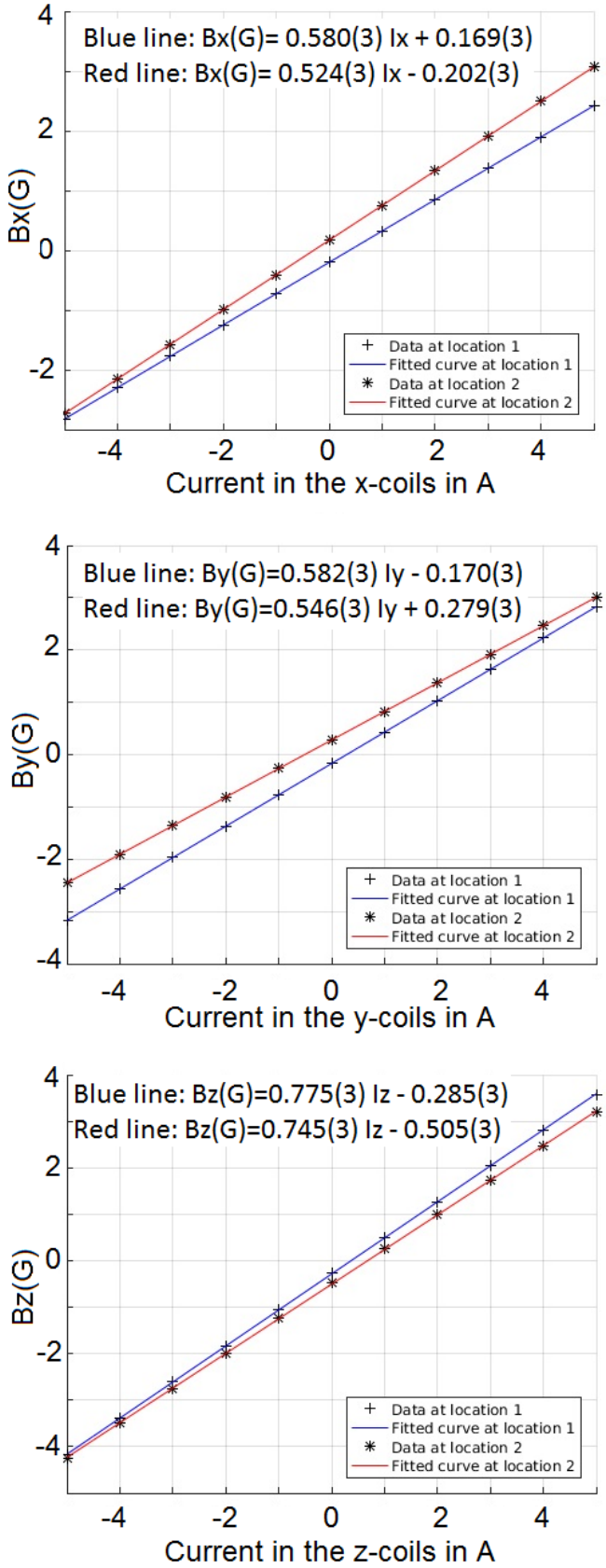

Figure 12: Magnetic field vs current in the x-, y- and z-direction at locations 1 and 2 (see Figure 10).

3.2 Determining the magnetic field gradient

The experimental set-up is placed on an iron table and the components are attached to the table with magnets. The experimental set-up has to be perfectly aligned, in order to prevent the components from shifting. However, the iron table might have an influence on the magnetic field. In order to determine this influence, the magnetic field was measured as a function of the height above the table.
A ruler was put in a holder at position 1 and 2. Near position 1 the magnetic field was measured at heights ranging from 0 cm to 16 cm at intervals of 2 cm. Then from 16 cm to 51 cm, at intervals of 5 cm. The same measurements were performed near position 2, except for the measurement at 51 cm, which was not deemed necessary, as the field did not vary strongly at this height. A Gaussmeter that could measure the total magnetic field and its x-, y- and z-component was used. A Matlab script was written to plot the data.

As can be seen in the graphs below, the x-, y- and z-component of the magnetic field at location 2 decreases linearly with the height, except for the value of the magnetic field at a height of 2 cm. This value is not taken into account for the fit and this deviation is due to the iron table. For location 1 there is no linear relation between the height and the magnetic field. The magnetic field is influenced by the turbo molecular pump (TMP). The TMP is used to obtain and maintain the vacuum in the vacuum chamber and is located close to location 1. A magnetic field of approximately 2 G was measured on top of the TMP. The TMP also explains the different offsets for the magnetic field at position 1 and 2 obtained in the previous experiment. The magnetic field contribution of the table becomes negligible at heights above 2 cm, based on the data from location 2.

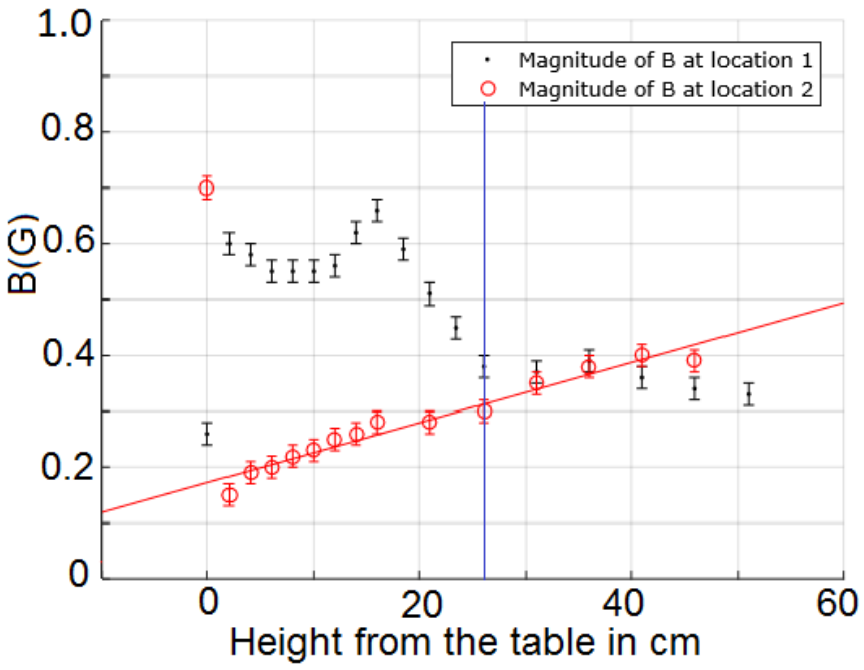

Figure 13: The total the magnetic field at location 1 and 2 as a function of height above the table (See Fig. 9). The vertical blue line at a height of 26 cm indicates the height of the Ba^+ ion

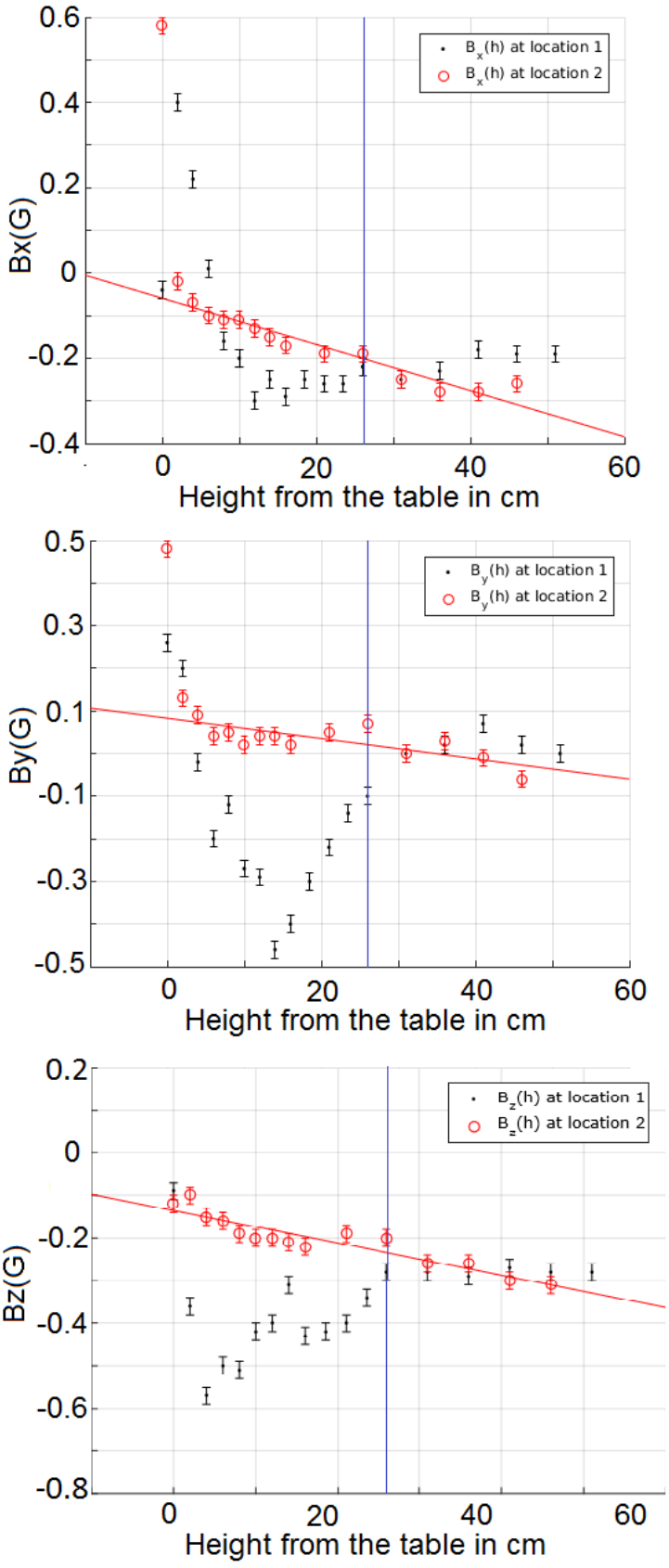

Figure 14: The x-,y- and z-component of the magnetic field at location 1 and 2 as a function of height above the table (See Fig. 9). The vertical blue line at a height of 26 cm indicates the height of the Ba^+ ion. The scale of the axes has been chosen for comparison.

3.3 Calibrating the magnetic field with trapped ions

Another way to calibrate the magnetic field at the position of the ion is to vary the magnetic field with ions inside the trap and to determine for what value of the magnetic field the count rate of the PMT has a minimum. The PMT measures the fluorescence light from the $6p^2P_{1/2}$- $6s^2S_{1/2}$ transition. The PMT count rate is reduced by dark states, states with a relatively long life time which are due to the forbidden transitions between two angular momentum eigenstates. The number of dark states depends on the difference ΔJ between the two states and the polarization of the laser light. A general discussion of the theory of dark states is given in [23]. In this measurement approximately 6 or 7 ions were trapped in a ion crystal and laser spectroscopy was performed. The frequency of the of the dye laser was detuned at -3 MHz and the frequency of the Ti:Sapphire laser was detuned at -75 Mhz in order to avoid Raman resonances in the measurement. With both the light shift laser and the spectroscopy laser on, the ions see a resulting laser field of both lasers and the polarization is randomized. There will be no dark states, so the count rate on the PMT is high. When the light shift laser is turned off, the PMT signal decreases. The polarization is no longer randomized and less transitions will occur. The count rate was measured while the direction and the magnitude of the magnetic field were varied. Since we see almost no signal at the PMT if the magnetic field is zero, we looked for a minimum in the PMT signal while the magnetic field in one direction was varied and the magnetic field in the other two directions was fixed. The total magnetic field is given by

$$|B| = \sqrt{(B_{x0} + c_x I_x)^2 + (B_{y0} + c_y I_y)^2 + (B_{z0} + c_z I_z)^2}, \tag{17}$$

where c_x, c_y and c_z are the gradients found in section 3.1 for the magnetic field dependence on the current in the x,y and z direction respectively. B_{x0},B_{y0} and B_{z0} are the residual magnetic fields we try to determine. The behaviour of this function is shown in Figure 14. For values of $(B_{z0} + c_z I_z)^2$ around zero the total magnetic field behaves as a quadratic function. For larger values of $(B_{z0} + c_z I_z)^2$ the total magnetic field behaves as a linear function. Since we want to determine for which current the residual magnetic field is compensated, we expect a quadratic behaviour of the count rate if we vary the magnetic field in one direction.

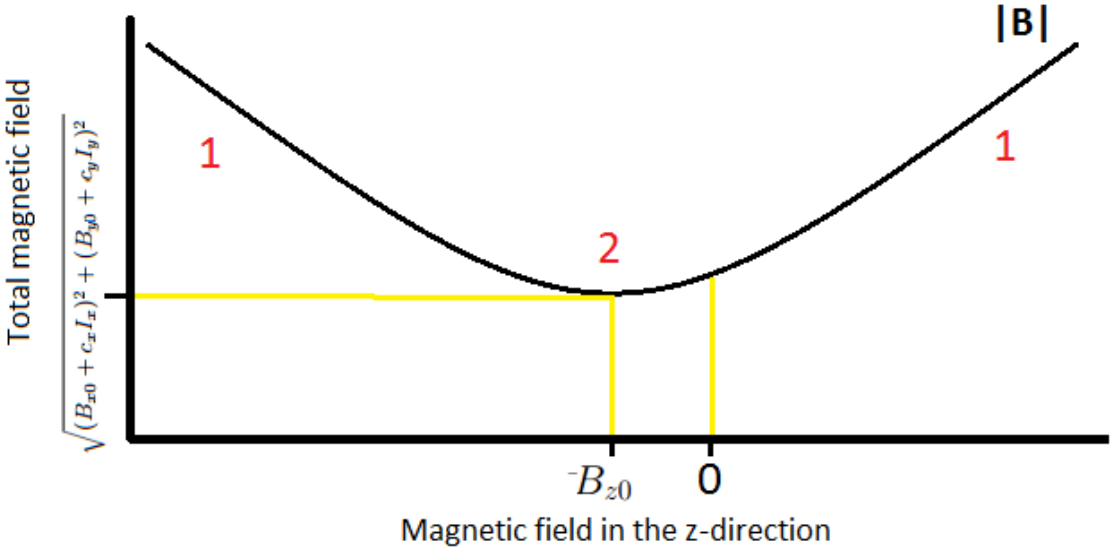

Figure 15: The total magnetic field as a function of the current on the coils in the z-direction. In regions 1 the current on the coils is large and the total magnetic field behaves as a linear function. In region 2 the z-component of the magnetic field is small and therefore the total magnetic field behaves as a quadratic function. The magnetic field in the z-direction is completely cancelled at the minimum of the total magnetic field at -B_{x0}. The same principle applies for the other two directions.

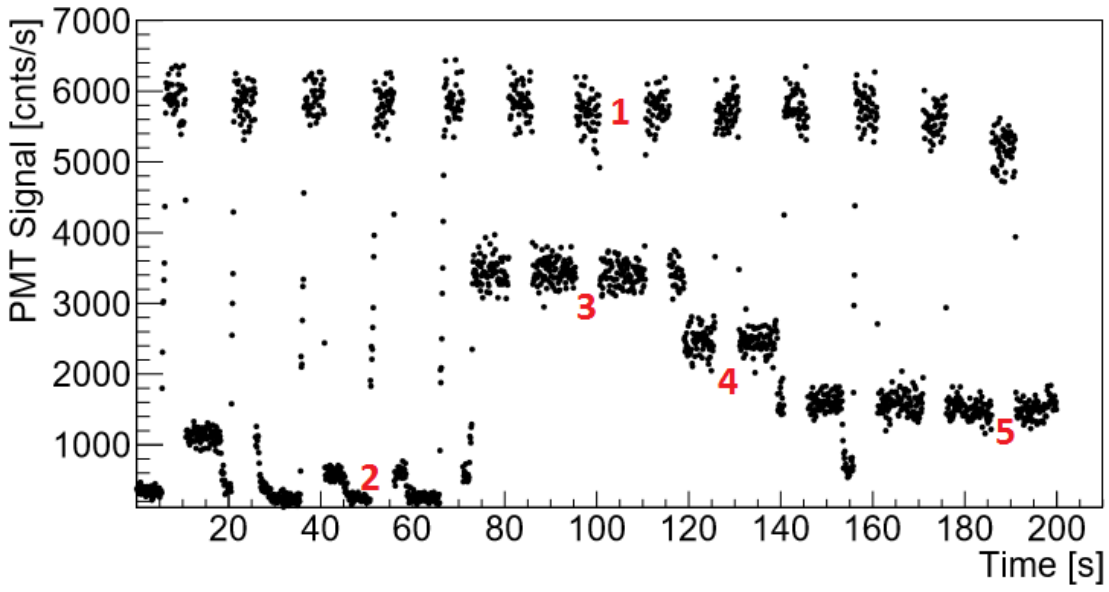

Figure 16: PMT signal vs Time. At 1 both the lasers are turned on and a lot of transitions occur. This is done to check whether the ion signal is not lost. In region 2 the ion signal was lost. In regions 3,4 and 5 the magnetic field in the z-direction was varied and different count rates are observed for different currents.

To be sure that the minimum in the count rate occurs because the ion is in a dark state and not because the ion signal is lost due to too much heating of the ion, both the light shift laser and spectroscopy laser are turned on for 5 seconds every 15 seconds. The other 10 seconds the light from the light shift laser is blocked and measurements can be performed to search for a minimum in the count rate. During the measurements, the total count rate obtained with both lasers turned on decreased by approximately 30 %, probably because some ions were lost in the process.

The PMT measures the fluorescence light from the $6p^2P_{1/2}$ - $6s^2S_{1/2}$ every 100 ms. As can be seen in Figure 18, the count rate distribution of the PMT signal is a Gaussian distribution. The uncertainty is given by the full width at half maximum (FWHM) dived by the square root of the number of counts. As indicated in the figure below, the FWHM has a value of 450 counts/s and the number of counts is approximately 300. The maximum is found at 3400 counts/s. Therefore, for the PMT signal we have

$$PMTSignal = (3400 \pm \frac{450}{\sqrt{300}})\frac{counts}{s} = 3400(26)\frac{counts}{s}. \quad (18)$$

Calculating this for every measurement would be a time-consuming activity and due to lack of time this was not done for every PMT value. Instead, the uncertainty for each PMT value was estimated by reading the highest and the lowest number of counts in the PMT Signal vs Time plots (Fig 16) and dividing that by 2. Since we measured the count rate without the light shift laser for 10 seconds and the PMT gives a 10 signals per second, there are 100 counts one measured interval. So for example for region 3 in Fig 14, we have approximately 300 counts.

The results have been plotted on the next page. The error in the PMT signal is too small to be observed in the plots.

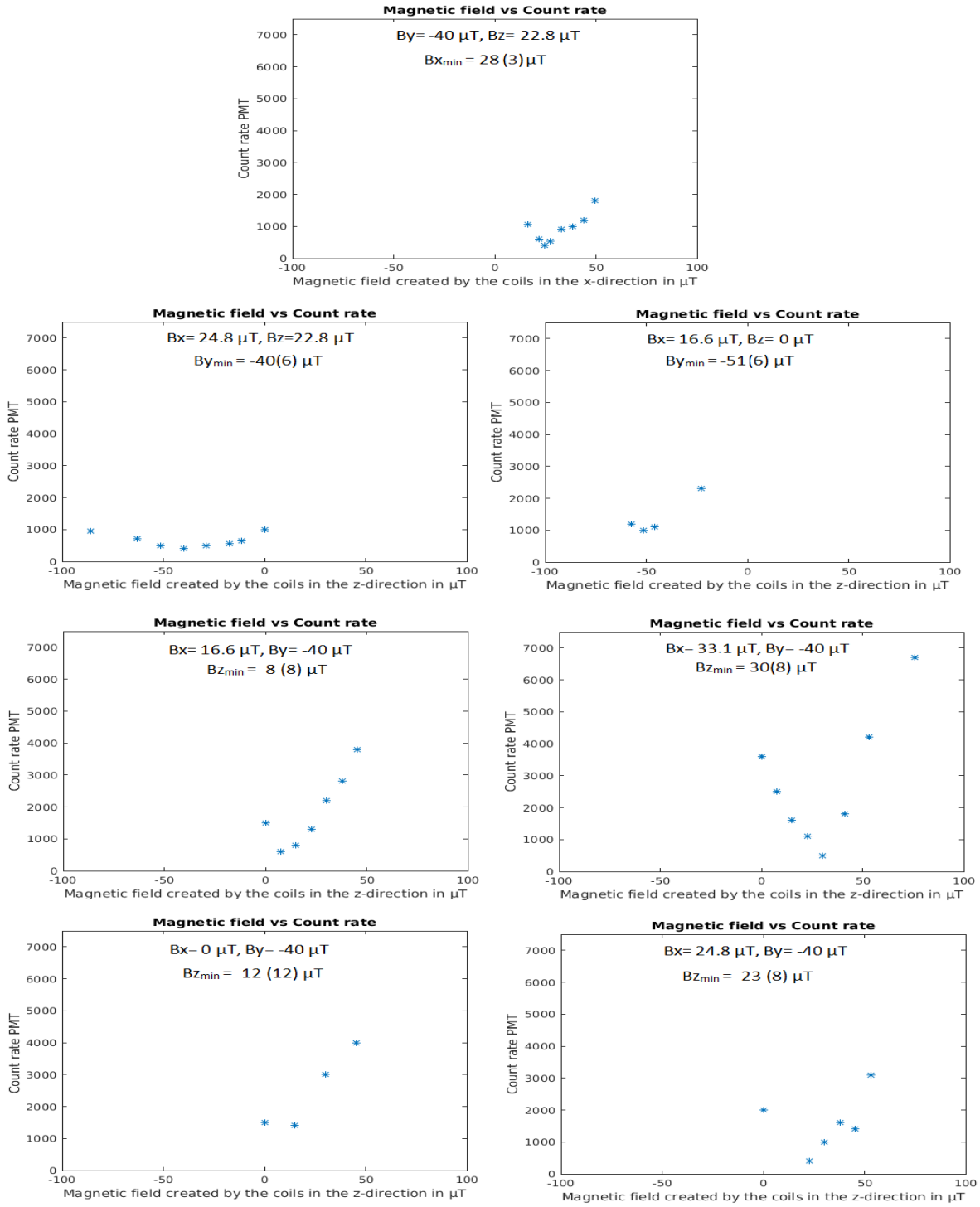

Figure 17: Count rate vs magnetic field in the x-, y- or z-direction. The magnetic field created by the square Helmholtz-like coil pairs in the other two directions is fixed and their values are displayed in the graphs. The minimums of the magnetic field in the x-, y- or z-direction are estimated from the data points.

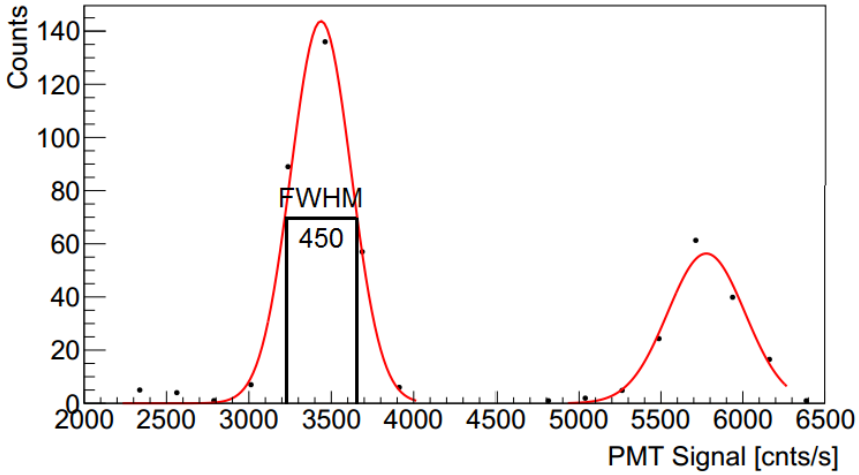

Figure 18: Number of counts vs PMT signal. The FWHM is indicated and the number of counts in this Gaussian distribution is approximately 300.

As can been seen, the photon scattering rate does not depend in a simple linear or quadratic way on the additional magnetic field created by the coils. A fit between the points has not been found and therefore minimums shown in the graphs are estimated. Take for example the graph on the top of Figure 18. The minimum has been found at 28 μT and the uncertainty has been estimated as half of the interval between the points on each side of the minimum. In this way the minimums are determined. More precision requires additional data points in the vicinity of the minimum. The values obtained are B_x= 28(3) μT B_y= -51(3)μT and B_y=-40(6) μT, B_z= 8(8) μT, B_z=12(12)μT, B_z=23(8)μT and B_z=30(8)μT. As can be seen from these results, the minimums in the count rate differ for different values of the magnetic field in the the two fixed directions. This can be explained by [23].

Berkeland and Boshier plotted the excited state population as a function of the magnetic field strength and the angle between the magnetic field and the polarization θ_{BE} for $^{88}Sr^{+}$ (Figure 19). The results are based on numerical solutions. Different detunings and polarizations have but used, but Berkeland and Boshier state in [23] that the resonance curve is not changed significantly even if the laser polarizations are perpendicular to each other or if the repumping laser is circularly polarized. Therefore, Figure 19 can be used to give a qualitative description of the population of the $^2P_{1/2}$ levels for our trapped Ba^+ ions.

The magnetic field components in two directions were fixed, while the magnetic field in one direction was varied. The total magnetic field is given by equation (15). Therefore, the angle between the magnetic field and our polarization, which is in the z-direction, is not constant and can be defined as

$$cos(\theta_{BE}) = \frac{B_z}{|B|} = \frac{B_{z0} + c_z I_z}{\sqrt{(B_{x0} + c_x I_x)^2 + (B_{y0} + c_y I_y)^2 + (B_{z0} + c_z I_z)^2}}. \quad (19)$$

So if the magnetic field in one direction is varied, the angle between the magnetic field and our polarization varies as well. For a small residual magnetic field the effect increases.

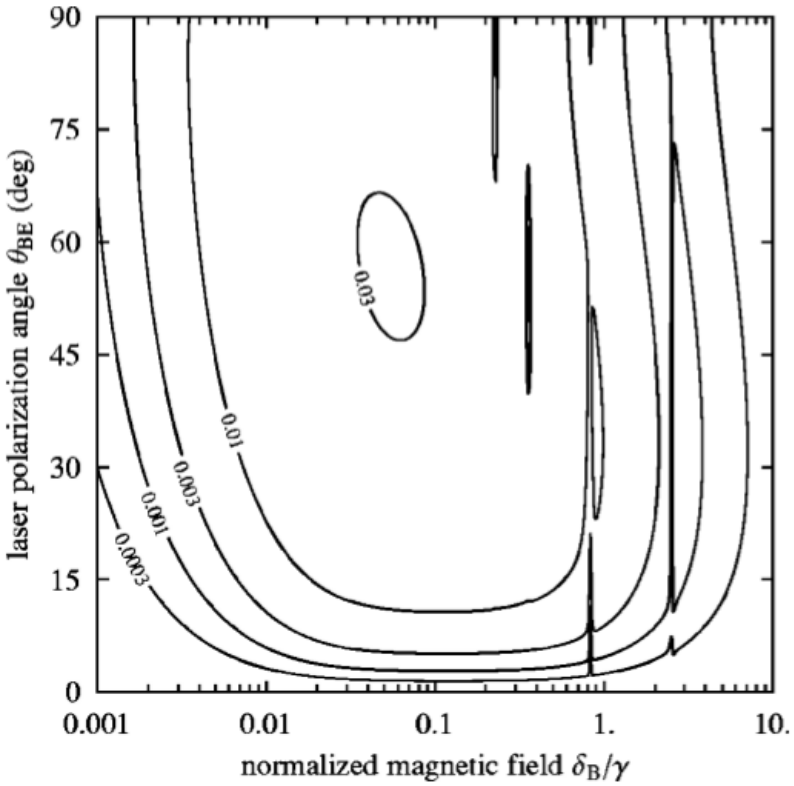

Figure 19: Population of the $^2P_{1/2}$ level of the $^{88}Sr^+$ $^2S_{1/2} \leftrightarrow {}^2P_{1/2} \leftrightarrow {}^2D_{3/2}$ system as a function of magnetic-field strength and of the angle between the magnetic field and the polarization vectors of the two laser fields. The detunings and resonant Rabi frequencies are given in terms of the excited state decay rate γ. The Rabi frequencies between the $^2S_{1/2}$ and $^2P_{1/2}$ state and the $^2P_{1/2}$ and $^2D_{3/2}$ are Ω_{SP}=Ω_{PD}=$(\sqrt{2}/5)$ γ. The detunings are $\Delta_{DP} = \gamma/2$ and $\Delta_{SP} = 0$. The narrow vertical features are dips due to Raman transitions. Different detunings and polarizations are used for this experiment than for our trapped Ba^+ ions, but simulations have shown that this does not change the curves significantly [23]. Therefore, this figure can be used to give a qualitative description of the population of the $6p^2P_{1/2}$ state for our trapped Ba^+ ions.

As can be seen in Figure 19, for a certain magnetic field strength and for different angles between the polarization and the magnetic field the population of the $^2P_{1/2}$ level differs. In our case the angle between the magnetic field and the polarization changes if the magnetic field in one direction is varied. Varying the magnetic field does not result a straight horizontal 'path' between the populations of the $^2P_{1/2}$ level, but in a curved path between the populations of the $^2P_{1/2}$ level. Since we vary the magnetic field in one direction around the minimum, this path is 'walked' back and forth. Therefore, the quadratic behaviour around the minimum for the magnetic field that was expected, is not observed and different minimums of the magnetic field in the direction that was varied, have been found for different values of the magnetic field that was fixed in the two other directions.

3.4 Angle measurements

It is desirable that the magnetic field points in a well defined direction. The direction of the magnetic field can be exploited to define the quantization axis of the ion. If the magnetic field is under an angle with the Ti:Sapphire and the dye laser beams, a combination of π- and σ-transitions will occur. In order to get only π- or σ-transitions, the magnetic field needs to be under a right angle with the Ti:Sapphire and the dye laser beams. To obtain a magnetic field that is perpendicular to the Ti:Sapphire and the dye laser beams, first the angle between the Ti:Sapphire and the dye laser beams has to be determined. This was done by hanging a plumb on the coil above the laser on both sides and measuring the distance between the plumb and the vacuum chamber. The diameter of the vacuum chamber was obtained from the drawings of the vacuum chamber. The angle β (see Figure 10) between the y-axis and the Ti:Sapphire and the dye laser beams was obtained by geometry

$$\beta = 7.0(2.1)^\circ. \tag{20}$$

The same procedure was executed for the angle α between the x-axis and the PMT/EMCCD

$$\alpha = 12.1(1.6)^\circ. \tag{21}$$

From the drawings of the vacuum chamber, the exact angle between the Ti:Sapphire laser and the dye laser beams and the PMT is 70.53 °. The angle obtained between the Ti:Sapphire and the dye laser beams and the PMT is 70.9(2.6) °.
The ratio between the current on the x-coils and y-coils for a magnetic field perpendicular to the Ti:Sapphire and the dye laser beams is

$$\frac{I_x}{I_y} = -8.5(3). \tag{22}$$

The detailed calculations are contained in Appendix A.

4 Discussion of the results

A relation between the currents in the square Helmholtz-like coils and the magnetic field induced in the x-, y- and z-direction was obtained with less than 1 % uncertainty and can be found in equations (9)-(11). The magnetic field gradient was determined to see if the iron table on which the vacuum chamber is placed, influenced the magnetic field. It was shown that this was not the case at the height from the table at the position of the ion (Figures 12 and 13). The values obtained for the magnetic field at zero current are B_x=1.6(3) μT, B_y=-5.4(3) μT and B_z=39.5(3) μT are influenced by magnetic field induced by the TMP at location 1 and are therefore not accurate. However, this did not influence the relation found between the currents in the square Helmholtz-like coils and the magnetic field induced in the x-, y- and z-direction. The magnetic field was calibrated with a trapped Ba^+ ion by varying the magnetic field in one direction with the magnetic field fixed in the other two directions and determining for which value of the magnetic field the count rate of the fluorescence light from the $6p^2P_{1/2}$- $6s^2S_{1/2}$ had a minimum. The values obtained are B_x=28(3) μT B_y=-51(3)μT and B_y=-40(6) μT, B_z=8(8) μT, B_z=12(12)μT, B_z=23(8)μT and B_z=30(8)μT. Because the population of the $^2P_{1/2}$ state depends on the relation between the strength of the magnetic field and the angle between the magnetic field and the polarization vector, which was not constant in our measurements, the minimums of the components of the magnetic field were not the same for different values of the magnetic field strength. This has only been described qualitatively. It is possible obtain a plot like Figure 19 for our Ba^+ ion, but this has not been performed. The ratio between the currents on the coils in the x- and y-direction to obtain a magnetic field that is perpendicular to the Ti:Sapphire and the dye laser beams is found with an uncertainty of 4 %, due to uncertainties in the measured distances, and is given by (22).

5 Conclusions

Measurements on the magnetic field inside three pairs of rectangular Helmholtz-like coils arranged in cubical geometry have been conducted and the following relations between the currents in the square Helmholtz-like coils and the magnetic field induced in the x-, y- and z-direction were obtained

$$B_x(I_x) = 5.52(3) \cdot 10^1 \mu T/A \cdot I_x - 0.16(3) \cdot 10^1 \mu T, \tag{23}$$

$$B_y(I_y) = 5.72(3) \cdot 10^1 \mu T/A \cdot I_y + 0.54(3) \cdot 10^1 \mu T, \tag{24}$$

$$B_z(I_z) = 7.60(3) \cdot 10^1 \mu T/A \cdot I_z - 3.95(3) \cdot 10^1 \mu T. \tag{25}$$

The values for the magnetic field with zero current, the background magnetic field, have been found but due to distortion of the magnetic field by magnetic components at one of the measuring points these values are not accurate.
The magnetic field gradient has been obtained to determine the influence of the iron table on which the the experimental set-up is placed. The influence of the iron table was only detectable directly on the table.
The magnetic field has been calibrated with a Ba^+ ion inside the trap by varying the magnetic field in one direction with a fixed magnetic field in the other two direction. Determined was for what value of the magnetic field components in the x-, y- and z-direction the count rate of the fluorescence light from the $6p^2P_{1/2}$- $6s^2S_{1/2}$ had a minimum. Due to the dependence of the population of the $^2P_{1/2}$ state on the relation between the strength of the magnetic field and the angle between the magnetic field and the polarization vector, the minimums obtained varied for different magnetic fields created by the coils in the two fixed directions. Further research has to be conducted to understand this dependence for a Ba^+ ion and to calibrate the magnetic field more accurate.
The angle αbetween the x-axis and the PMT/EMCCD and the angle β between the y-axis and the Ti:Sapphire laser beam and the dye laser beam have been determined as $\alpha = 12.1(1.6)^\circ$ and $\beta = 7.0(2.1)^\circ$. From these angles the ratio between the currents on the coils in the x- and y-direction to obtain a magnetic field that is perpendicular to the Ti:Sapphire and the dye laser beams is determined as

$$\frac{I_x}{I_y} = -8.5(3). \tag{26}$$

.

Appendices

A Details of the experiments geometry

To survey the geometry of the experiment, distances were measured with a plumb hanging down from the outer side of the coils. A ruler was used to measure the distances between the tip of the plumb and the vacuum chamber. The diameter of the vacuum chamber was obtained from the drawings of the vacuum chamber and is 25.6 cm. The distance between the coils was measured with a tape measure. The coils had a diameter of 1.5 cm. Since the distances were measured between the outer sides of the coils and between the centers, 1.5 cm has been subtracted from the distance.

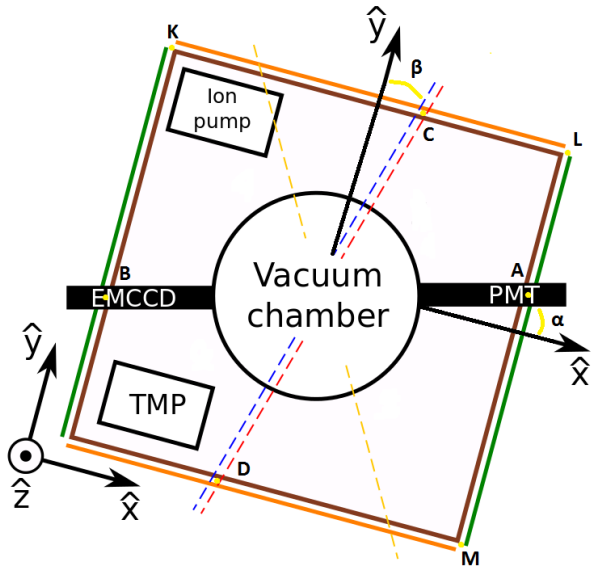

Figure 20: Schematic description (top view) of the experimental set up. PMT stands for Photo Multiplier Tube and EMCCD for Electron Multiplying CCD and both are used for the imaging of the ions. The yellow line is the light shift laser, the blue and red laser are for the cooling of the ion and the laser spectroscopy. The green and yellow lines indicate the rectangular current coils. The angles α and β are between the x-axis and the EMCCD/PMT as well as the y-axis and the direction of the Ti:Sapphire and dye laser beams respectively The characters A up to and including M are used to define distances [16].

Distance $|AB| = 67.5(3)$ cm and distance $|CD|$=66.5(3) cm.

The distance $|KL| = |LM|$= 66.0 cm.

From the cosine rule follows then that the angle α between the x-axis and the PMT/EMCCD is

$$\alpha = 12.1(1.6)^\circ. \tag{27}$$

The angle β between the y-axis and the Ti:Sapphire and the dye laser beams is

$$\beta = 7.0(2.1)^\circ. \tag{28}$$

The uncertainty follows from [24]

$$\delta\beta = \sqrt{\left(\frac{\delta\beta}{\delta|CD|}\right)^2 \cdot (\Delta|CD|)^2}, \tag{29}$$

where

$$\beta = \cos^{-1}(\frac{|LM|}{|CD|}) \tag{30}$$

and

$$\frac{\delta\beta}{\delta|CD|} = \sqrt{\frac{|LM|}{|CD| \cdot \sqrt{(|CD|)^2 - (|LM|)^2}}}. \tag{31}$$

Filling in the distances obtained gives the error in the angle β in rad. By replacing $|CD|$ for $|AB|$ the same was done for the angle α.

To determine the ratio between the current on the coils in the x- and y-direction for which the magnetic field is perpendicular to the Ti:Sapphire land the dye laser beams, the following must hold by geometry

$$\vec{B} = \frac{\text{-}B_y}{cos\beta} = \frac{B_x}{sin\beta}. \tag{32}$$

This gives

$$\vec{B} = \frac{\text{-}B_y}{B_x} = \frac{cos\beta}{sin\beta} = 0.123(5). \tag{33}$$

The uncertainty follows from [24]

$$\Delta(\frac{\text{-}B_y}{B_x}) = \sqrt{(\frac{\delta(\frac{\text{-}B_y}{B_x})}{\delta\beta})^2 \cdot (\Delta\beta)^2} \tag{34}$$

with

$$\frac{\delta(\frac{\text{-}B_y}{B_x})}{\delta\beta} = \frac{1}{cos^2(\beta)}, \tag{35}$$

where $\beta = 7.0\ ^\circ$ and $\Delta\ \beta = 0.037$ rad.
The expressions for B_x and B_y as a function of the current were determined as

$$B_x(I) = 5.52(3) \cdot 10^{-1} G/A, \tag{36}$$

$$B_y(I) = 5.72(3) \cdot 10^{-1} G/A. \tag{37}$$

Inserting this in (33) gives

$$\frac{\text{-}B_y}{B_x} = \frac{-5.72(3) \cdot 10^{-1} G/A \cdot I_y}{5.52(3) \cdot 10^{-1} G/A \cdot I_x} = 0.123. \tag{38}$$

Solving for I_x gives

$$I_x = -8.5(3) \cdot I_y. \tag{39}$$

The error follows from [24]

$$\Delta I_x = \sqrt{(\frac{\Delta(\frac{\text{-}B_y}{B_x})}{(\frac{\text{-}B_y}{B_x})})^2 \cdot (I_y)^2} \tag{40}$$

So we obtain for the ratio $\frac{I_x}{I_y}$

$$\frac{I_x}{I_y} = -8.5(3). \tag{41}$$

6 Acknowledgements

I would like to thank my supervisors prof. dr. Klaus Jungmann and dr. Lorenz Willmann for all their help and the time they took to answer my questions. I would like to thank Sietse Buijsman for the good times of working in the laboratory together on the first two measurements described in this thesis. Amita and Elwin, thank you for helping me with the measurements in the laboratory and with analyzing the results.

References

[1] Robert Oerter. The theory of almost everything, Pearson Eduction, Inc. 2006.

[2] Mayerlin Nuñez Portela. Single ion spectroscopy in preparation of an atomic parity violation measurement in ra^+, Thesis, Rijksuniversiteit Groningen, 2014.

[3] R.W. Hayward D.D. Hoppes C.S. Wu, E. Ambler and R. P. Hudson. Experimental test of parity conservation in beta decay, Phys. Rev. Lett., 105(4):1413-1415, 1957.

[4] Kurt Sundermeyer. Femtosecond laser spectroscopy, Springer Cham Heidelberg New York Dordrecht London, 2014.

[5] L. Wansbeek. Atomic parity violation in a single trapped radium ion, Thesis, Rijksuniversiteit Groningen, 2011.

[6] G.S. Giri. Radium ion spectroscopy towards atomic parity violation in a single trapped ion, Thesis, Rijksuniversiteit Groningen, 2011.

[7] John C. Morrison. Modern physics for scientists and engineers, Elsevier, 2010.

[8] Alan Corney. Atomic and laser spectroscopy, Oxford Scholarship online, 2007.

[9] H.S. Lee H. Davoudiasl and W.J. Marciano. Dark z implications for parity violation, rare meson decays, and higgs physics, Phys.Rev.D, 85:115090, 2012.

[10] M. A. Bouchiat and C. Bouchiat. Parity violation induced by weak neutral currents in atomic physics .1, J. De Physique, 35(12):899–927, 1974.

[11] J. J. Curry. Compilation of wavelengths, energy levels, and transition probabilities for ba i and ba ii, Journal of Physical and Chemical Reference Data, 33(3):725–746, 2004.

[12] Jeffrey A. Sherman. Single barium ion spectroscopy: light shifts, hyperfine structure, and progress on an optical frequency standard and atomic parity violation y, University of Washington, 2007.

[13] David J. Griffiths. Introduction to quantum mechanics, Pearson Education, Inc. , 2005.

[14] Nadia Röck. Quantum manipulation on the barium quadrupolar transition, University of Innsbruck, Thesis, 2011.

[15] Joel Hussels. Light shift in ba^+ and ra^+ ions, Bachelor Thesis, RUG, 2014.

[16] S. Buijsman. Investigating the effect of external magnetic fields and polarisation of intense light fields on ba^+ ions, Bachelor Thesis, RUG, 2016.

[17] Anthony E. Siegman. Lasers, University Science Books, 1986.

[18] Jay E. Newman. Physics 100 laser theory, http://minerva.union.edu/newmanj/Physics100/, 2014.

[19] P. Luc S. Gerstenkorn. Atlas du spectre d'absorption de la molecule d'iode, 14800-20000 cm^{-1}, Labaratoire Aim$'e$ Cotton, CNRS II, Orsay(France), 1978.

[20] Jun Ye (edited by Peter Hannaford). Femtosecond laser spectroscopy, Springer Science+Business Media, Inc, 2005.

[21] Carlos R. Pinedo-Jaramillo Andres F. Restrepo Alvarez, Edinson Franco-Mejia. Study and analysis of magnetic field homogeneity of square and circular helmholtz coil pairs: A taylor series approximation, ANDESCON '12 Proceedings of the 2012 Andean Region International Conference,Pages 77-80 , 2012.

[22] Figure made by Elwin Dijck, van Swinderen Institute, Groningen, Netherlands, 2016.

[23] D. J. Berkeland and M. G. Boshier. Destabilization of dark states and optical spectroscopy in zeeman-degenerate atomic systems, Physycal Review A, 65(3):033413 , 2002.

[24] Vern Lindberg. Uncertainties and error propagation part 1 of a manual on uncertainties, graphing, and the vernier caliper, url: *http : //www.rit.edu/ w-uphysi/uncertainties/Uncertaintiespart2.html*, 2001.